B. Zheng[1]

H. J. Wang[2]

Q. L. Wang[2]

R. Kovacevic[1]

[1] Southern Methodist University, Dallas, TX 75275
[2] Harbin Institute of Technology, Harbin 150001, P.R. China

Imaging the Keyhole in PAW of Aluminum Alloys

This paper presents a technique for front image sensing of the weld pool in variable polarity plasma arc welding of aluminum alloys, and describes the determination of the geometrical size of the keyhole for subsequent real-time feedback control of a full penetration weld. Image formation occurs when the arc light reflects off the concave mirror-like surface of the depressed keyhole weld pool, and passes through a band-pass filter onto the image sensor. The image of the visual keyhole (nominal keyhole) is a two-dimensional projected picture of the actual keyhole weld pool. The variation in area of the nominal keyhole is closely correlated with the variation of the bottom width of the weld bead.

1 Introduction

Variable polarity plasma arc welding (VPPAW) of aluminum alloys in the keyhole mode has been successfully used in production [1–4]. However, selecting process parameters and providing control during welding to produce a satisfactory weld remains a challenge. One effective approach is to monitor the keyhole weld pool. Recently, it was found that the presence or absence of a keyhole can be determined by measuring the ratio of hydrogen to argon in the plasma arc column with an optical spectrometer [5]. However, the size of the keyhole can not be determined. At present, two difficult problems are associated with top face sensing of the keyhole weld pool in PAW: inaccessibility of the weld pool because of the limited torch stand-off distance and the interference of the arc radiation. PAW technology in the one-keyhole-per-pulse mode can be fairly well applied to steels, so the arc sound or the arc efflux light from the backside of the workpiece can be used to detect the size of the keyhole. Based on this principle, a full penetration weld bead has been guaranteed in real-time feedback control [6–9]. However, this type of technology is not applicable to VPPAW of aluminum alloys. Also, detecting the keyhole from the backside of the workpiece is not feasible in some cases, such as in the welding of pressure tanks. To date, constant parameter open loop control of weld formation is still being used in PAW of aluminum alloys by the keyhole mode.

In recent years, welding researchers have focused on using machine vision systems to sense the weld pool for controlling the full penetration state in gas tungsten arc welding (GTAW) and gas metal arc welding (GMAW) [10–15]. The arc light filtering solution has been investigated by Richardson and coworkers through coaxial viewing of the weld pool in GTAW [16]. These approaches are based on the principle that the diffuse reflection of arc light from the mirror-like weld pool surface is weaker than that from the surrounding area. Thus, in the image, the weld pool produces a dark area, while the solid part of the workpiece appears as a bright area. Kovacevic and coworkers used a pulsating laser synchronized with a high-shutter-speed camera to overcome the arc light interference in GTAW of stainless steel [17–19]. With this approach, a clear image of the weld pool is captured and the weld pool boundary is calculated in real-time using a developed image processing algorithm. The geometrical appearance of the weld pool is characterized with the rear angles and the length of the weld pool. For the full penetration case, the root surface weld bead width could be determined using the pool area and a ratio of a surrounding area of the pool to the weld pool area. Chin and coworkers extensively investigated infrared thermography [20–22]. It was found that the interference of the bright arc light could be avoided, and the depth of the joint penetration could be determined using the characteristics of the temperature profiles in GTAW of steel. The instantaneous decrease of the welding current has also been used to weaken the intensity of the arc light in order to capture a clear weld pool image during welding [23]. However, in some cases, this approach may not be acceptable due to the poor weld bead that occurs, such as in PAW of aluminum alloys using the keyhole mode.

Besides the inaccessibility of the weld pool and the arc radiation interference in PAW, a common problem existing in welding of aluminum alloys is that nearly no color change occurs when the plate is melted. Consequently, the molten weld pool can not be easily distinguished from the solid base metal using the visible spectrum range. Thus, processing a weld pool image for the case of aluminum alloys is much more difficult than in the case of steel welding.

Therefore, this study was undertaken to investigate (1) the feasibility of front image sensing of the keyhole weld pool of aluminum alloys, (2) the physics of the image formation of the nominal keyhole, and (3) the relationship between the keyhole geometry and weld bead width.

2 Experimental Procedure

Experimental System. The image sensing system used for this investigation is shown in Fig. 1. It consists of a band-pass filter, a CCD camera, a monitor, an image processing card, a PC-Pentium computer, and a video recorder. The parameters of the filter are the following: center wave length 658 nm, half wave width 10 nm, transmissivity 27 percent, and background depth of field 1/1000. These specific filter parameters are selected because the intensity of the arc light when using argon as the shielding gas is much weaker within the above spectrum. The welding system shown in Fig. 2 consists of a variable polarity welding power source, programmable sequence controller, plasma gas controller, CNC positioning system, wire feeder and plasma arc torch. The camera is attached to and positioned in front of the plasma arc torch with its axis at an angle ϕ from the workpiece surface plane.

Experimental Conditions. Variations in the keyhole size can be induced by changing some of the welding conditions, such as the welding current, the shape of the workpiece plates and the wire feeding speed. Bead-on-plate welds are made without wire feeding. Two shapes of 5.0 mm-thick 2024 aluminum plates are shown in Fig. 3. The welding current in the startup segment reaches 90 A within 5.0 seconds, which increases up to 120 ~ 150 A within 5.0 ~ 10.0 seconds from the termination of this segment to the beginning of the main body segment. Other parameters have the following values: a DCEN (direct current electrode negative) to

Contributed by the Manufacturing Engineering Division for publication in the JOURNAL OF MANUFACTURING SCIENCE AND ENGINEERING. Manuscript received Nov. 1997; revised Dec. 1998. Associate Technical Editor: S. Kapoor.

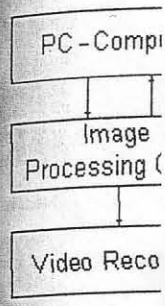

Fig. 1 Block diagram of pool

DCEP (direct current el
ms, DCEN current 120
plasma gas flow rate 3.0
welding speed 100.0 m
angle of workpiece surf
85 deg, orifice diamete
tungsten electrode setba

3 Image Features

Keyhole Profile. Ir
age, a three-dimensiona
4. The keyhole is actua
profile resembling a tru
both in diameter and sha
sectional diameter occu
section diameter). The
located about 1.5 mm ~
workpiece (throat secti
section on the bottom su
diameter, but less than
welding without wire fe

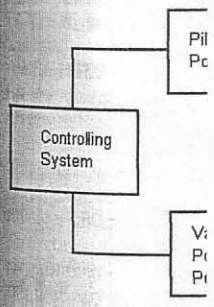

Fig. 2 Block diagram of

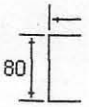

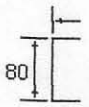

Fig. 3

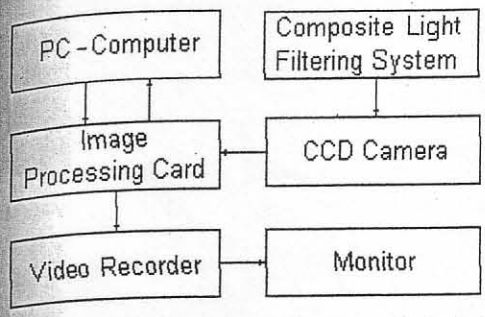

Fig. 1 Block diagram of the image sensing system for keyhole weld pool

DCEP (direct current electrode positive) time ratio of 22 ms to 3.0 ms, DCEN current 120 ~ 150 A, DCEP current 150 ~ 180 A, plasma gas flow rate 3.0 L/min., shielding gas flow rate 5.0 L/min., welding speed 100.0 mm/min., torch stand-off distance 5.0 mm, angle of workpiece surface plane to the horizontal plane equal to 85 deg, orifice diameter 4.0 mm, orifice length 4.0 mm, and a tungsten electrode setback 4.0 mm.

3 Image Features of the Keyhole Weld Pool

Keyhole Profile. In order to better understand a keyhole image, a three-dimensional schematic of a keyhole is shown in Fig. 4. The keyhole is actually a cave through the weld pool, with a profile resembling a trumpet. The cross section of this cave varies both in diameter and shape (irregular ellipse). The maximum cross sectional diameter occurs at the top surface of the workpiece (top section diameter). The cross section with the smallest diameter is located about 1.5 mm ~ 2.5 mm up from the bottom surface of the workpiece (throat section diameter). The diameter of the cross section on the bottom surface of workpiece is larger than the throat diameter, but less than the top section diameter. In vertical-up welding without wire feeding, the shape of a backside weld bead

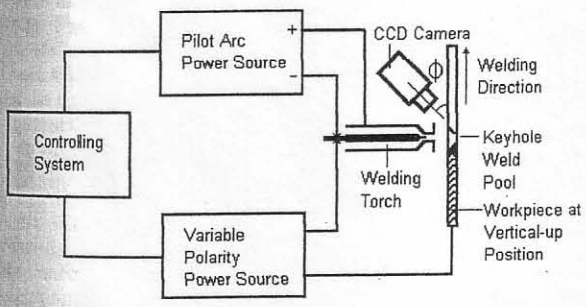

Fig. 2 Block diagram of variable polarity plasma arc welding system

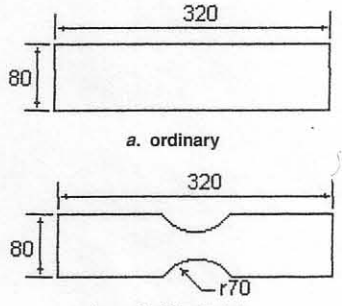

Fig. 3 Schematic of workpieces

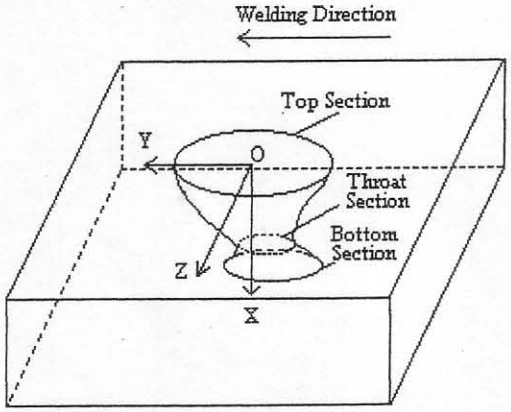

Fig. 4 Three dimensional schematic of a keyhole

is concave-downwards along the entire weld path (see Fig. 5). Therefore, the keyhole weld pool is a deformed weld pool, and is much different from a weld pool in GTAW and GMAW [17–19].

Image Features of the Keyhole Weld Pool. Images of a keyhole weld pool are shown in Fig. 6, the schematic of which is shown in Fig. 7. The main features of the image are as follows.

(1) The images are two-dimensional profiles of the keyhole weld pools projected onto the target plane of the camera, which is defined in this paper as the visual (nominal) keyhole weld pool. This means that only a single viewpoint of the keyhole weld pool can be captured by the camera, and the curves in the image are generally in different spatial planes. The pattern of the keyhole weld pool in the image is deformed with respect to the pattern of the actual keyhole weld pool.

(2) The front periphery S of the nominal keyhole weld pool is clear, but the portion of it at the location with the largest weld bead width can not be clearly distinguished from the solid area of the

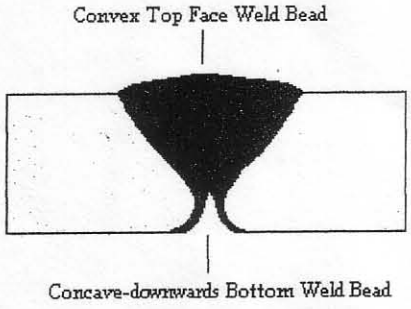

Fig. 5 Schematic of the cross section of weld bead without wire feeding

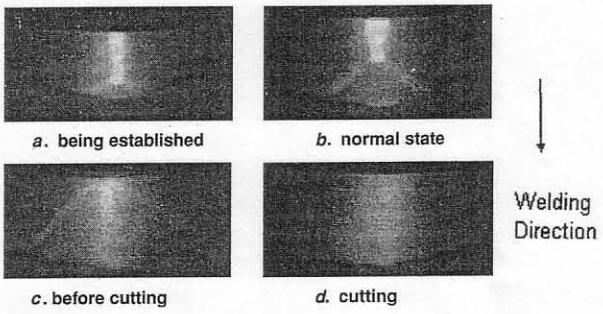

Fig. 6 Images of the sensed keyhole weld pool with varied welding current

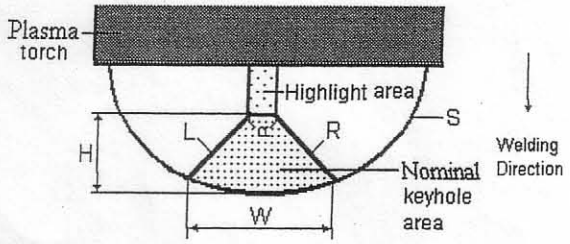

Fig. 7 Schematic of the nominal keyhole weld pool viewed from the top face weld

base metal. The rear periphery of the nominal keyhole weld pool can not be seen in the image.

(3) The lines L and R are projected lines of the actual periphery of the keyhole. They may be the periphery of the keyhole throat (at the throat cross section, see Fig. 4). However, the periphery S is on the workpiece surface. So, actually, the three curves (L, R and S) are not in the same spatial plane (L and R are not parallel to the workpiece surface). The area, bounded by lines L and R and the periphery S, is a type of keyhole area, through which the plasma arc goes. This area is defined in this paper as the nominal keyhole.

(4) A highlighted area behind the nominal keyhole exists in the image during a normal welding process. The highlighted area is not the image of the bright arc, but the reflected light from the arc on the rear surface of the weld pool. The area of the nominal keyhole will increase with an increase in welding current, but the highlighted area will decrease with an increase in welding current. This is because the size of the actual keyhole increases. The area of the nominal keyhole increases to a maximum until the highlighted area vanishes (because there is no surface to reflect the arc light) when the welding process becomes the cutting process.

(5) The bright arc cone can not be seen directly from the image because of the shielding of the torch gas cup.

4 Reason for the Image Formation of the Keyhole Weld Pool

The image of a keyhole weld pool is actually a reflecting image. The concave-downwards and mirror-like surface of the keyhole weld pool reflects the light from the plasma arc onto the target plane of the camera. The following factors will influence the intensity of the image: the arc light strength and its distribution along the plasma arc column, the surface shape of the keyhole weld pool, the filtering parameters, and the angle between the camera and the workpiece surface plane. Because the arc is strongly constricted when it passes through the orifice of the nozzle, the portion of the plasma arc cone at the exit of the orifice is very bright. However, the portion of the plasma arc column away from the orifice exit is much less intense. Under the conditions of this paper, the outer gas cup of the plasma arc torch blocks the arc cone portion that could cause image interference.

The formation of the highlighted area in the image is related also to the position of the arc cone and the deformation of the keyhole weld pool. Since the torch standoff distance is about 5.0 mm, the bright arc cone is actually a light source over the keyhole weld pool. The light is projected onto the rear mirror-like surface of the deformed keyhole weld pool, and then reflected onto the target plane of the camera. In order to better understand the formation of the highlighted area, the hole through the solid crater in the end of the keyhole weld bead is chosen to approximately represent the dynamic keyhole since the profile of the keyhole can not be currently measured during welding. To form a mold and obtain a profile of the keyhole after welding, the following steps were taken: (1) fill the hole with liquid glue; (2) cut the workpiece and remove the solidified glue block; (3) take the image of the solidified glue block using a CCD camera and transfer it into a computer image processing system; (4) draw the block profile, as shown in Fig. 8 (relative to the actual position in Fig. 2, the drawing in Fig. 8 is rotated counterclockwise 85 deg into the horizontal position). The curve Y_1 (the front longitudinal outline of the keyhole), the angle θ_1 (between the normal of each point on Y_1 and the workpiece surface plane), the curve Y_2 (the back longitudinal outline of the keyhole) and the angle θ_2 (between the normal of each point on Y_2 and the workpiece surface plane) can be expressed as follows:

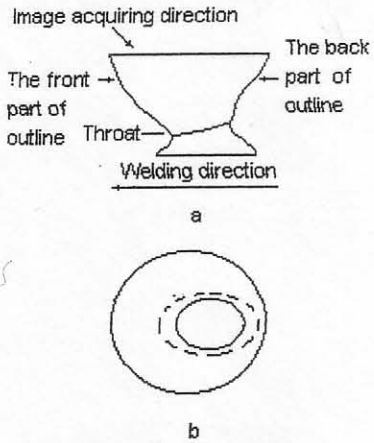

Fig. 8 View of the keyhole weld pool
a. front view b. top view

$$y_1 = 0.29 + 1.56x - 0.19x^2 + 0.022x^3 - 1.20E - 3x^4 + 3.52E - 5x^5 - 6.47E - 7x^6 \quad (1\text{-}1)$$

$$\theta_1 = \text{arctg}\,(-1/(1.56 - 0.38x + 0.066x^2 - 4.80E - 3x^3 + 1.76E - 4x^4 - 3.88E - 6x^5)) \quad (1\text{-}2)$$

$$y_2 = 249.294 + 0.97E - 3x - 0.09x^2 + 0.06x^3 - 2.58E - 4x^4 + 6.13E - 6x^5 - 8.94E - 8x^6 \quad (1\text{-}3)$$

$$\theta_2 = \text{arctg}\,(-1/(2.97E - 3 - 0.18x + 0.18x^2 - 103E - 3x^3 + 3.05E - 5x^4 - 5.36E - 7x^5)) \quad (1\text{-}4)$$

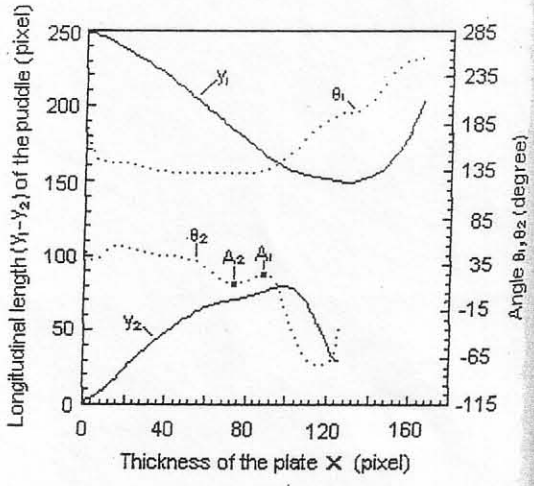

Fig. 9 Schematic of the profiles of the weld pool and their angles of the normal to the workpiece plane

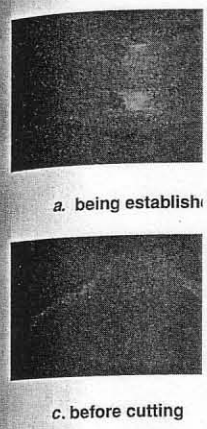

a. being establish

c. before cutting

Fig. 10 Images of the r current

Where E equals 2.718 ness o. he workpiece.

The four curves bas 9 (30 pixels in length = two breaks, A_1 and A_2, to the throat of the key deg ~ 25 deg. Hence, nearly the same as the the area of the keyhole concave mirror-like s projects the light onto nearly equal to ϕ. The weld pool results from

There is only one la exposure of the camera smaller separate highli of the keyhole and the when the exposure is confirmed by analyzir shown in Fig. 6.

The front periphery smooth surface of pu metal. However, the br hit the target plane of different from the angl

It can be seen from throat is a spatial curv it can be assumed to b throat plane), which is Since the solid base m the front part of the thr the rear part of the thr plasma arc torch. Co throat can be seen in t throat is also a mirro

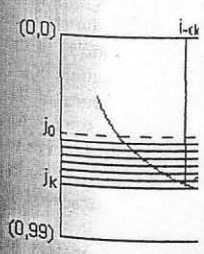

Fig. 11 Schematic of

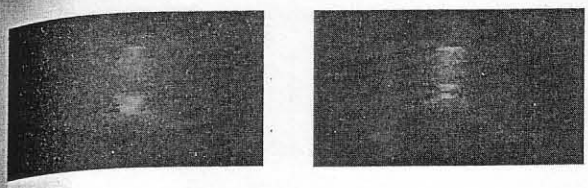

a. being established

b. normal state

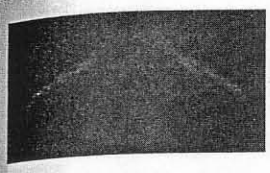

c. before cutting

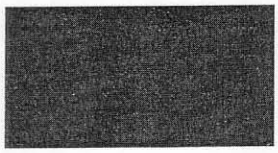

d. cutting

Fig. 10 Images of the nominal keyhole weld pool with varied welding current

Where E equals 2.71828 and x is the coordinate along the thickness of the workpiece.

The four curves based on the above formulas are shown in Fig. 9 (30 pixels in length = 1.0 mm). It can be observed that there are two breaks, A_1 and A_2, in the curve of angle θ_2, which are adjacent to the throat of the keyhole. The range of variation in θ_2 is only 15 deg ~ 25 deg. Hence, the average value of θ_2 is 20 deg, which is nearly the same as the angle ϕ (20 deg). It could be deduced that the area of the keyhole weld pool between A_1 and A_2 is actually a concave mirror-like surface where the arc light is focused. It projects the light onto the target plane of the camera at an angle nearly equal to ϕ. The highlighted area in the image of the keyhole weld pool results from this reflecting arc light.

There is only one large highlighted area in the image when the exposure of the camera is intense (Fig. 6). However, there are two smaller separate highlighted areas in the image, one near the throat of the keyhole and the other near the top surface of the workpiece, when the exposure is weak (Fig. 10). This phenomenon was also confirmed by analyzing the different gray values in the images shown in Fig. 6.

The front periphery of the keyhole weld pool in the image is a smooth surface of pure metal with a very thin layer of melted metal. However, the bright arc cone light reflected from it does not hit the target plane of the camera because the reflecting angle is different from the angle ϕ. Thus, its gray level in the image is low.

It can be seen from Fig. 8*a* that the periphery of the keyhole throat is a spatial curve (not in the same spatial plane). However, it can be assumed to be in the same plane (defined in the paper as throat plane), which is at an angle to the workpiece surface plane. Since the solid base metal in front of the keyhole weld pool blocks the front part of the throat plane in the direction of the camera, only the rear part of the throat can be viewed from the front side of the plasma arc torch. Consequently, only part of the rear keyhole throat can be seen in the image. The periphery of the rear keyhole throat is also a mirror-like surface of molten liquid, which can

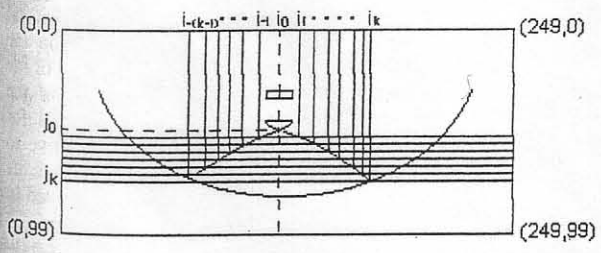

Fig. 11 Schematic of the periphery tracing for the nominal keyhole

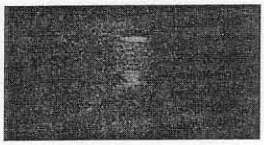

a. original image

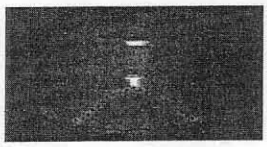

b. processed image

Fig. 12 Original and processed images of the nominal keyhole weld pool

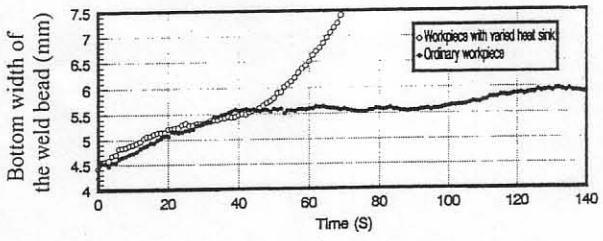

a

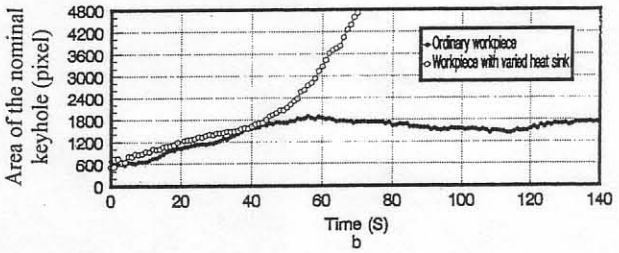

b

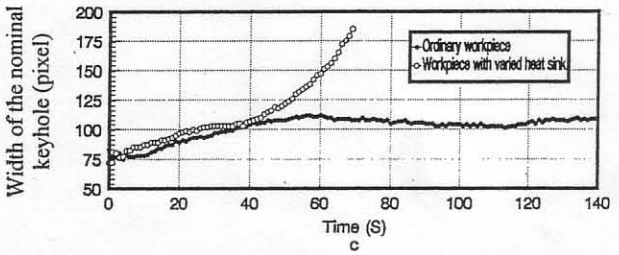

c

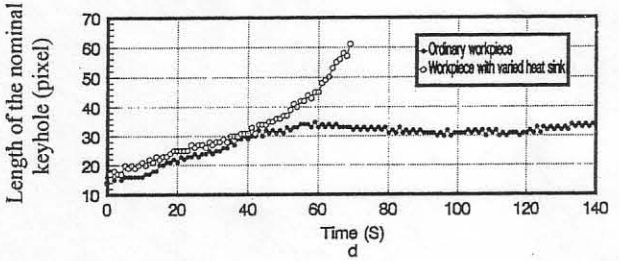

d

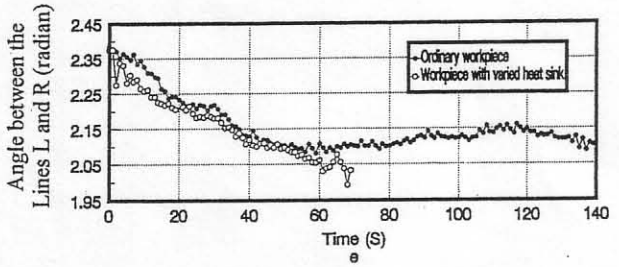

e

Fig. 13 Geometrical sizes of the bottom weld bead and the nominal keyhole versus welding time

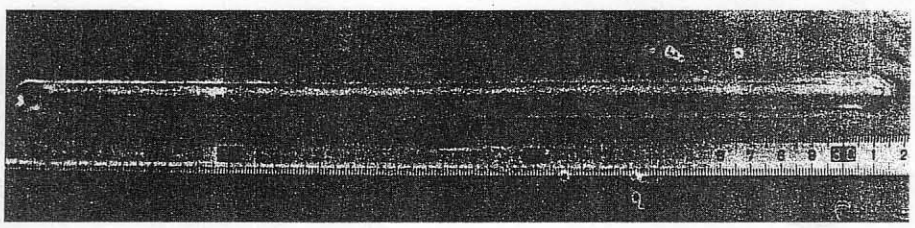

a. front side

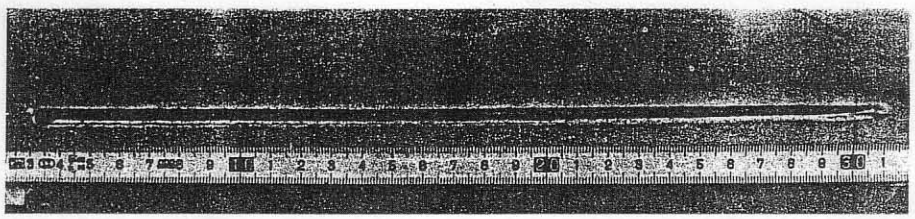

b. back side

Fig. 14 Photographs of the weld bead with the ordinary workpiece

reflect the light of the bright arc cone towards the camera. Thus, its gray level intensity in the image is high, but lower than that of the highlighted area. The periphery of the rear keyhole throat consists of two straight lines (L and R) with an acute angle between them, but not a smooth arc line. The reason for this is that the backside weld bead is concave-downwards (see Fig. 5).

5 Extracting the Nominal Keyhole Periphery

Since the image of the nominal keyhole weld pool is clear and the difference in grayness between the periphery of the nominal keyhole and the other area is large, no image preprocessing is needed. The characteristic points and the lines of the nominal keyhole can be directly extracted, as shown in Fig. 11.

The periphery of the nominal keyhole is determined as follows. (1) Find the vertical centerline of the highlighted area in the image. (2) Determine the starting point for tracing the periphery of the nominal keyhole. (3) Trace the periphery of the nominal keyhole. (4) Determine the front periphery of the nominal weld pool.

One of the processed images of the nominal keyhole is shown in Fig. 12*b*.

6 The Geometrical Sizes of the Nominal Keyhole and Discussion

Based on the results of the processed images, the variations over time in some of the geometrical features of the nominal keyhole, such as the area, the width (W), the length (L) and the angle (α) of the periphery of the nominal keyhole (see Fig. 7), are investigated. In order to determine if the geometrical features of the nominal keyhole in the image could reflect the variation of the weld formation during welding, the bottom widths of the weld bead are measured manually. The corresponding curves are shown in Fig. 13, in which the origin of the time axis represents the instant when the workpiece movement begins after the keyhole size reaches a certain value.

(1) The bottom width of the weld bead on the ordinary workpiece increases with time during the first 40 seconds (Fig. 13*a*). At the instant following keyhole formation, it is about 4.3 ~ 4.4 mm due to the better heat transfer conditions of the workpiece at the beginning of welding. At 40 seconds, it increases to 5.6 mm, and remains almost unchanged because of the constant heat sink. However, at 120 seconds, it slightly increases to 5.9 mm because of the poor heat transfer conditions at the end of the workpiece. Therefore, the bottom weld bead width varied approximately 0.3 mm and remains almost uniform while the heat sink is constant (see Fig. 14). When the workpiece with the variable heat transfer condition is used, the bottom width of the weld bead sharply increases at 44 seconds due to the poor heat sink. At 70 seconds, it increases to 7.5 mm. Thus, it varies about 2.0 mm during this period. Actually, from the corresponding photos of the weld bead in Fig. 15, it can be seen that at about 70 seconds, the welding process changes into a cutting process. Therefore, the transition from a normal welding process to a cutting process occurs after 26 seconds, and the corresponding variation in the bottom weld bead width is 2.0 mm.

(2) The variations in the area, width and length of the nominal keyhole (Fig. 13(*b–d*), respectively) obtained from the image are in close agreement with that of the bottom width of the weld bead. However, the above-mentioned geometrical features of the nominal keyhole will remain constant after 48 seconds. The varied magnitudes of the area, width and length of the nominal keyhole with the ordinary workpiece are respectively 400 pixels, 12 pixels and 14 pixels once the heat sink of the workpiece becomes constant in the welding process. However, for the varied heat sink workpiece, the corresponding geometrical features increase from 1800 pixels, 104 pixels and 30 pixels at the 40 second mark to 4800 pixels, 184 pixels and 60 pixels at the 70 second mark when the welding process becomes the cutting process. Therefore, the corresponding time interval between the welding process and the cutting process is about 20 seconds according to the size of the nominal keyhole in the image. However, the angle between the line L and the line R (Fig. 13*e*) with the varied heat sink workpiece does not reflect the variation in the bottom width of the weld bead.

(3) The changes in the area, width and length of the nominal keyhole in the image accurately represent the variations in the bottom width of the weld bead, regardless of the magnitude of the variation or the instant of occurrence. These dimensions of the nominal keyhole can be used as the characteristic signals for avoidance of the cutting process. The area is more sensitive to changing welding conditions than the width and length. Thus, its degree of variation is much greater than the changes observed in the width and length.

(4) The time interval required for the welding process to become the cutting process shows that the response time for both

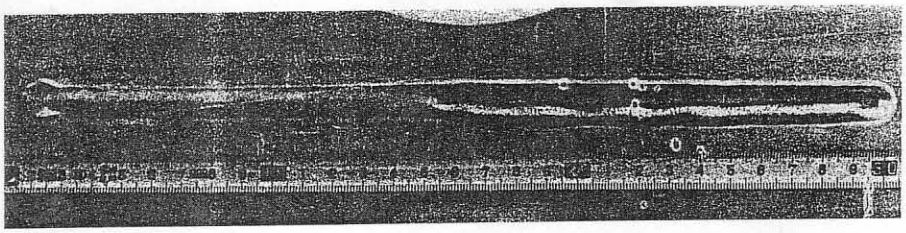

a. front side

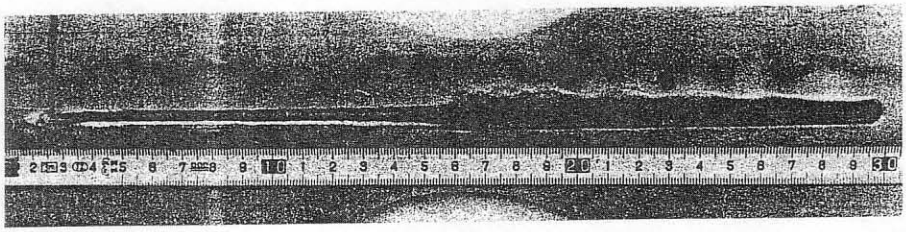

b. back side

Fig. 15 Photographs of the weld bead with the varied heat sink workpiece

acquiring and processing of the image and for control of the keyhole should be less than 20 seconds.

Conclusions

The following conclusions can be made based on the results of this study:

(1) A band-pass filter is used to obtain a clear image of the keyhole weld pool. The nominal keyhole in the image is a part of the actual keyhole, the geometrical features of which reflect the variation in the bottom width of the weld bead.

(2) The area of the nominal keyhole extracted by the developed image processing algorithm can be used as a characteristic parameter to monitor and control the weld formation.

(3) The image formation of the actual keyhole is closely related to the concave-downwards mirror-like surface of the weld pool, the camera position, and the arc cone light.

Acknowledgment

The authors wish to thank the National Key Laboratory of Advanced Welding Production Technology, Harbin Institute of Technology, P. R. China and Southern Methodist University, Dallas, TX for financial support.

References

1 Nunes, A. C., "Variable Polarity Plasma Arc Welding on Space Shuttle External Tank," *Welding Journal,* 1984, Vol. 63, No. 4, pp. 27–35.

2 Howard, Woodward, "A U.S. Contractor for the International Space Station," *Welding Journal,* 1996, No. 3, pp. 35–40.

3 Torres, M. R., "Gas Contamination Effects in Variable Polarity Plasma Arc Welded Aluminum," *Welding Journal,* 1992, Vol. 4, pp. 123–130.

4 Martinez, Luis F., "Effect of Weld Gases on Melt Zone Size in VPPA Welding of Al 2219," *Welding Journal,* 1994, No. 10, pp. 50–55.

5 Martinez, L. F., "Front Side Keyhole Detection in Aluminum Alloys," *Welding Journal,* 1992, No. 5, pp. 49–52.

6 Steffens, H. D., "Automatic Control for Plasma Arc Welding with Constant Keyhole," *Welding Journal,* 1972, No. 6, pp. 40–45.

7 Metcalfe, J. C., and Quigley, M. B. C., "Keyhole Stability in Plasma Arc Welding," *Welding Journal,* 1975, No. 11, pp. 401–404.

8 Zhang, J. H., and Wang, Q. L., "Study on Arc Sound in TIG and Plasma Processes," IIW Doc. 212-610-85, 1985, 7.

9 Hu, B. X., "The Study of Controlling System of Welding Quality at All-Position by Using the Arc Sound in Pulsed Plasma Arc Welding of Steel," *Welding,* 1980, Vol. 3, pp. 17–20.

10 Agapakis, J. E., and Bolstad, J., "Vision Sensing and Processing System for Monitoring and Control of Welding and Other High Luminosity Processes," *International Robots & Vision Automation Conference,* 1991, pp. 23–29.

11 Nakata, S., Huang, J., and Tsuruha, Y., "Visual Sensing System for In-Process Control of Arc Welding Process," *Welding International,* 1988, No. 12, pp. 1086–1090.

12 Hoffman, T., "Real-Time Imaging for Process Control," *Advanced Materials & Processes,* 1991, No. 9, pp. 37–43.

13 Guu, A. C., and Rokhlin, S. I., "Computerized Radiographic Weld Penetration Control with Feedback on Weld Pool Depression," *Materials Evaluation,* 1989, No. 10, pp. 1204–1210.

14 Guu, A. C., and Rokhlin, S. I., "Arc Weld Process Control Using Radiographic Sensing," *Materials Evaluation,* 1992, No. 11, pp. 1344–1348.

15 Rokhlin, S. I., and Guu, A. C., "Computerized Radiographic Sensing and Control of an Arc Welding Process," *Welding Journal,* 1990, Vol. 69, No. 3, pp. 83–95.

16 Richardson, R. W., and Gutow, D. A., "Coaxial Arc Weld Pool Viewing for Process Monitoring and Control," *Welding Journal,* 1984, Vol. 63, No. 3, pp. 43–50.

17 Kovacevic, R., and Zhang, Y. M., "Three-dimension Measurement of Weld Pool Surface," *International Conference on Modeling and Control of Welding Processes,* Florida, 1993.

18 Kovacevic, R., and Zhang, Y. M., "Vision Sensing of 3D Weld Pool Surface," *The 4th International Conference on Trends in Welding Research,* Gatlinburg, 1995.

19 Kovacevic, R., and Zhang, Y. M., "Monitoring of Weld Penetration Based on Weld Pool Geometrical Appearance," *Welding Journal,* 1996, Vol. 10, pp. 317–329.

20 Nagarajan, S., Chen, W. H., and Chin, B. A., "Infrared Sensing for Adaptive Arc Welding," *Welding Journal,* 1989, Vol. 68, No. 11, pp. 462–466.

21 Nagarajan, S., Banerjee, P., Chen, W. H., and Chin, B. A., "Weld Pool Size and Position Control Using IR Sensors," *Proceedings of NSF Design and Manufacturing Systems Conference,* Arizona State University, 1990.

22 Chen, W., and Chin, B. A., "Monitoring Joint Penetration Using Infrared Sensing Techniques," *Welding Journal,* 1990, Vol. 69, No. 4, pp. 181s–185s.

23 Oshima, K., and Morita, M., "Sensing and Digital Control of Weld Pool in Pulsed MIG Welding," *Transactions of the Japan Welding Society,* 1992, Vol. 23, No. 4, pp. 36–42.